nature nanotechnology
SUPPLEMENTARY INFORMATION
DOI: 10.1038/NNANO.2013.272

Efficient solar water-splitting using a nanocrystalline CoO photocatalyst

Longb Liao, Qiuhui Zhang, Zhihua Su, Zhongzheng Zhao, Yanan Wang, Yang Li, Xiaoxiang Lu, Dongguang Wei, Guoying Feng, Qingkai Yu, Xiaojun Cai, Jimin Zhao, Zhifeng Ren, Hui Fang, Francisco Robles-Hernandez, Steven Baldelli and Jiming Bao

(1) Synthesis of CoO powders

Co_3O_4 powders (Sigma-Aldrich, purity 99.99%, size < 10 μm,) were decomposed into CoO powders in a quartz tube furnace at 1000 °C in an Ar environment (99.999% purity). The tube was pumped by a mechanical pump to ~50 mTorr after the loading of Co_3O_4 powders. Ar was then flowed at 240 sccm to fill the tube to ambient pressure, and this Ar flow rate and 1 atm pressure were kept for the duration of the synthesis. The tube was heated from room temperature (25 °C) to 800 °C in 1/2 hr and from 800 °C to 1000 °C in 2 hrs. The furnace was then kept at 1000 °C for 10 hrs and then cooled at the following rates: 1000 °C to 900 °C in 1/2 hr and 900 °C to room temperature in 10 hrs. Figure S1 shows initial Co_3O_4 powders and converted CoO powders.

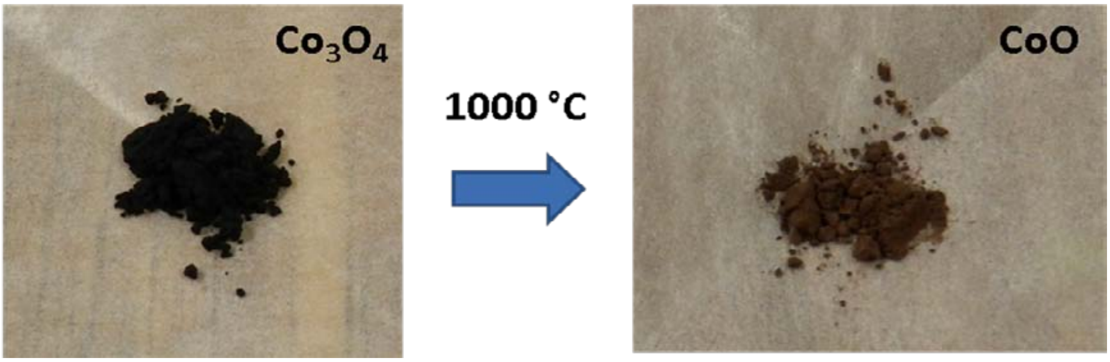

Figure 1. The conversion of black Co_3O_4 to brown CoO powders through thermal decomposition.

(2) Synthesis of CoO nanoparticles or nanocrystals

CoO micropowders were ablated by femtosecond laser pulses in pure water (molecular biology reagent, Sigma-Aldrich) in a 10 mL beaker. 150 fs laser pulses from Spectra-physics Hurricane were centered at 805 nm with an average power of 375 mW at 1 KHz repetition rate. A lens with f = 20 cm was used to focus laser pulses on CoO micropowders. The generated CoO nanoparticles (nanocrystals) became suspended in the water, and were collected directly for water-splitting experiments. A Sampleprep 8000M Mixer/Mill from SPEX was used to turn CoO micropowders to nanoparticles. Such generated particles have a wide distribution of particle sizes. In order to selected nanoparticles, the milled particles were dispersed in pure water, smaller size nanoparticles were selected using centrifugation.

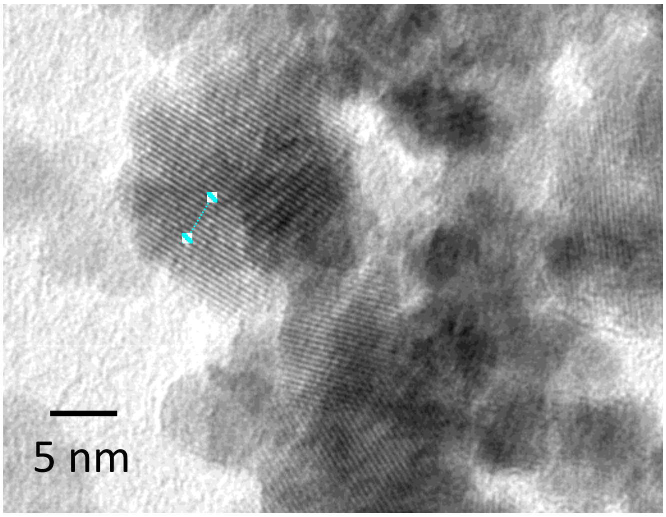

Figure 2. High resolution TEM image shows lattice fringes of CoO nanocrystals. The line connecting two white squares indicates the line scan shown in Supplementary Fig. 3.

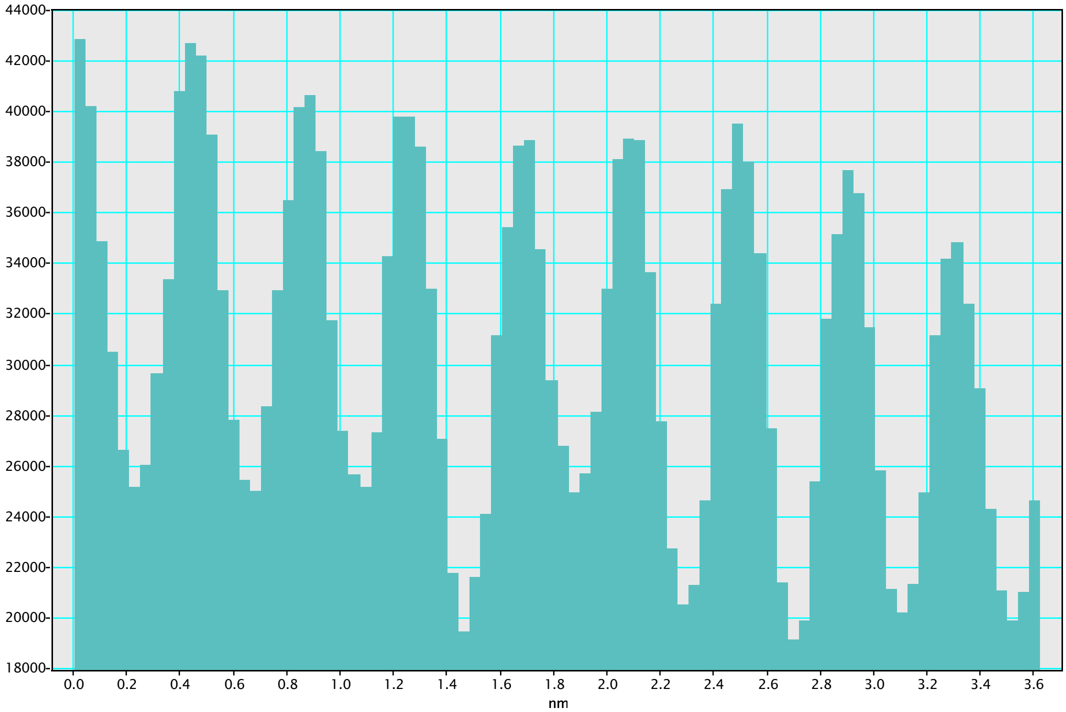

Figure 3. Line scan of TEM lattice fringe (Supplementary Fig. 2) confirms 0.41 nm lattice constant of cubic CoO.

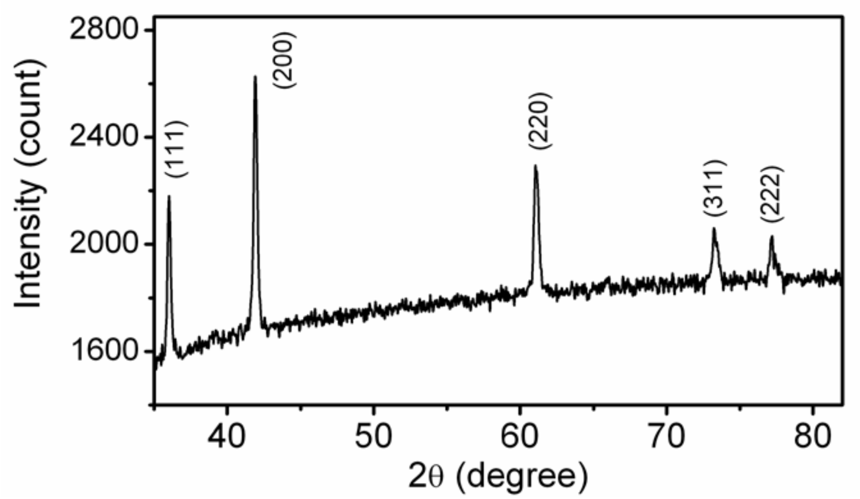

Figure 4. Typical XRD spectrum of CoO nanoparticles.

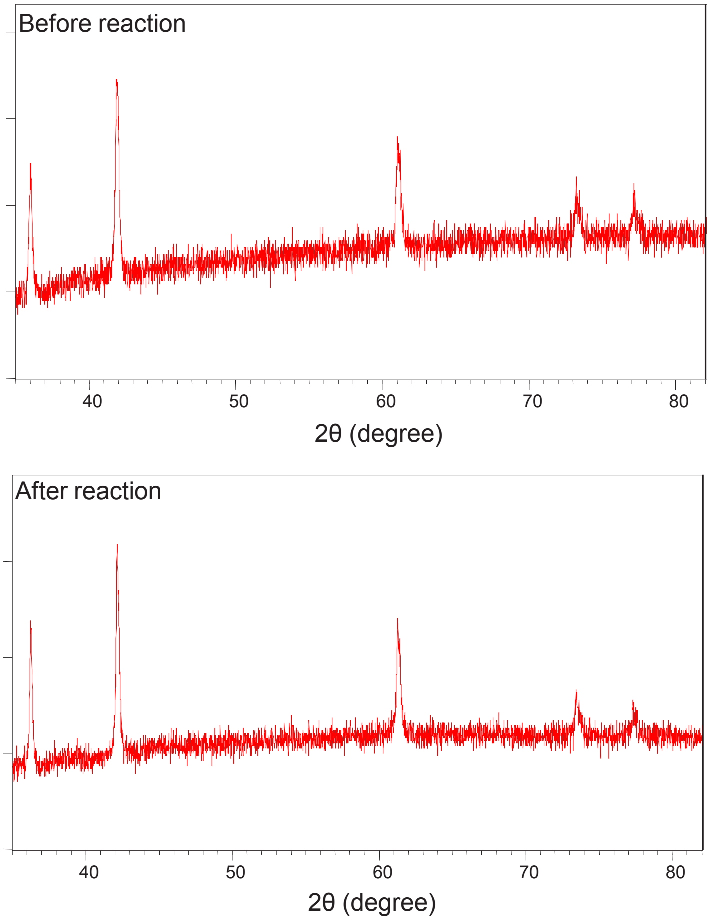

Figure 5. XRD spectra of same CoO nanoparticles (top) before and (bottom) after photocatalytic reaction.

DOI: 10.1038/NNANO.2013.272

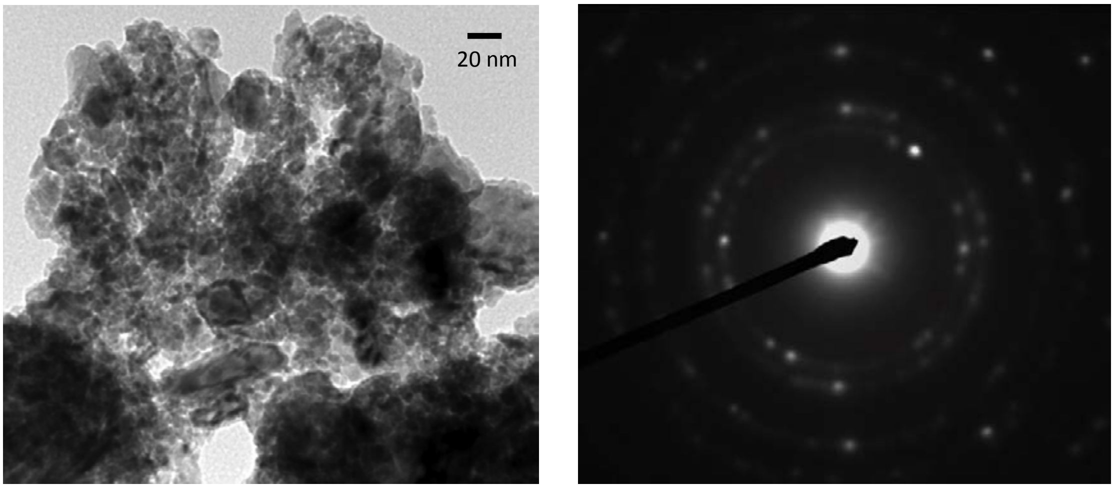

Figure 6. TEM image and diffraction of CoO nanoparticles after photocatalytic water-splitting.

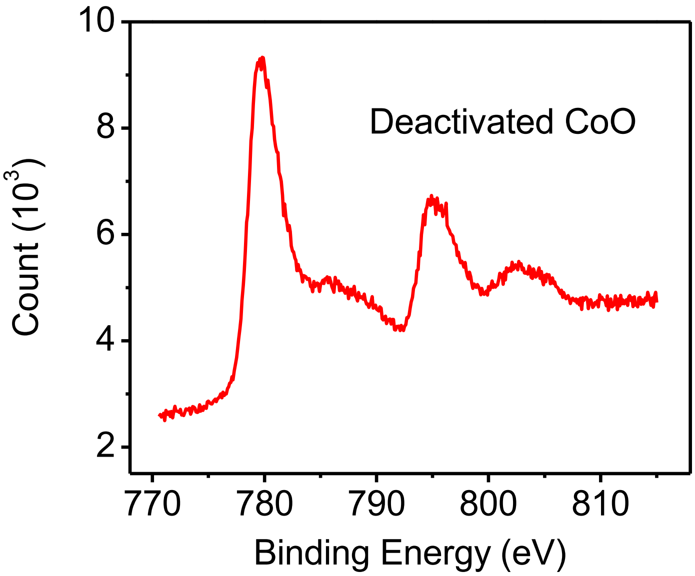

Figure 7. XPS spectrum of CoO nanoparticles after photocatalytic water-splitting.

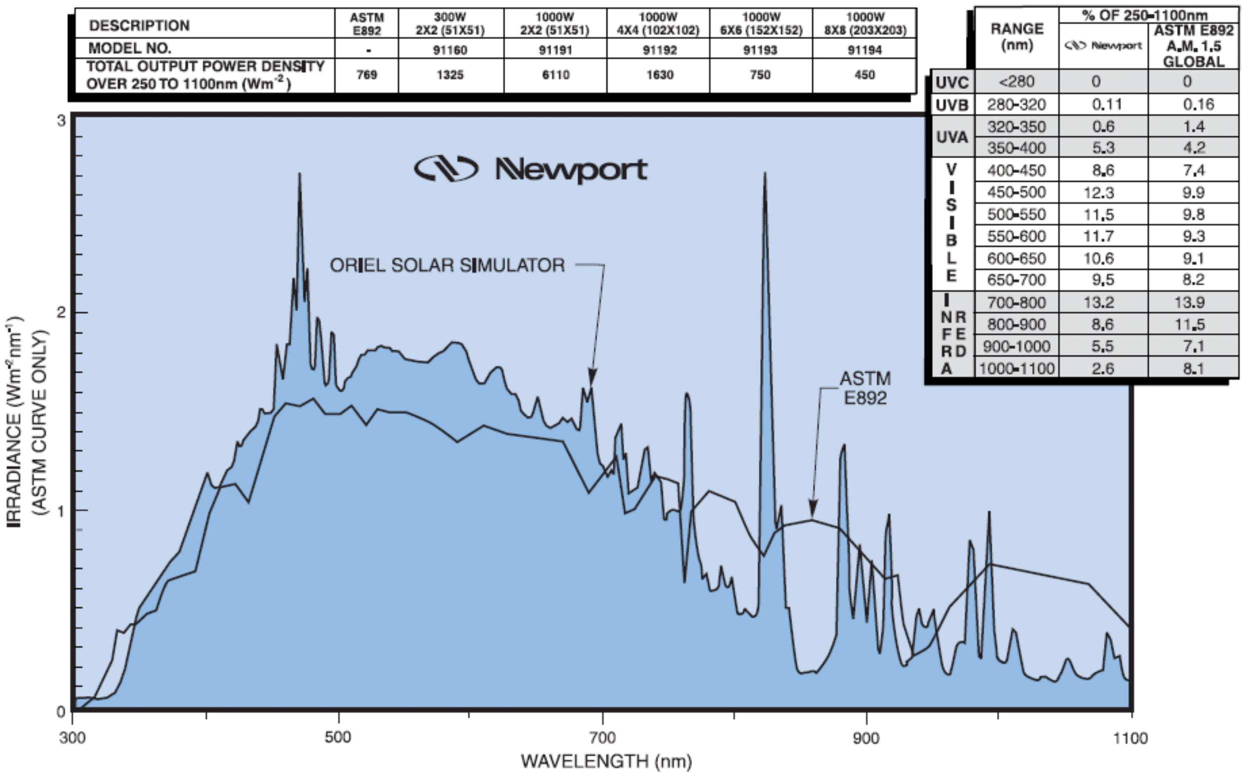

DESCRIPTION	ASTM E892	300W 2X2 (51X51)	1000W 2X2 (51X51)	1000W 4X4 (102X102)	1000W 6X6 (152X152)	1000W 8X8 (203X203)
MODEL NO.	-	91160	91191	91192	91193	91194
TOTAL OUTPUT POWER DENSITY OVER 250 TO 1100nm (Wm^{-2})	769	1325	6110	1630	750	450

	RANGE (nm)	% OF 250-1100nm	
		Newport	ASTM E892 A.M. 1.5 GLOBAL
UVC	<280	0	0
UVB	280-320	0.11	0.16
UVA	320-350	0.6	1.4
	350-400	5.3	4.2
VISIBLE	400-450	8.6	7.4
	450-500	12.3	9.9
	500-550	11.5	9.8
	550-600	11.7	9.3
	600-650	10.6	9.1
	650-700	9.5	8.2
INFRARED	700-800	13.2	13.9
	800-900	8.6	11.5
	900-1000	5.5	7.1
	1000-1100	2.6	8.1

Figure 8. Typical output spectral distribution of Oriel AM 1.5 Global Simulators normalized to the ASTM E892 standard spectrum.

(3) CoO Nanoparticles used in the experiments

CoO nanoparticles synthesized by ball milling were used in the experiments shown in the following figures:

Figures 1b and 1c, Figures 2a and 2b, supplementary figures 2-3, 6-7.

CoO nanoparticles synthesized by laser ablation were used in the experiments shown in the following figures:

Figure 1a, figures 2c and 2d, figures 3a-c, supplementary figures 4-5.

(4) Home-built system to identify and quantify gas species from ^{18}O-labeled water splitting

The system is shown in Fig. S9. It consists of a gas sampling chamber (~33 mL in volume) connected to a high vacuum chamber through a gas leak valve. The gas sampling chamber is pumped to ~30 mTorr. The high vacuum chamber is equipped with a mass spectrometer (SRS RGA200), and is pumped to 10^{-7} Torr continuously by a turbo molecular pump. Gas samples from the syringe are injected into the gas sampling chamber through an injection port. After injection of gas, the pressure of the gas sampling chamber increases, gas molecules will diffuse to the high vacuum chamber through the leak valve, and are detected by the RGA. The higher the gas pressure in the gas sampling chamber, the larger the gas RGA partial pressure will be. However, because hydrogen has a higher diffusion constant than oxygen through the leak valve, the RGA will give a larger hydrogen vs oxygen signal than their actual pressure in the gas sampling chamber, as shown in Fig. 2c-d. In order to quantitatively obtain an accurate H_2 to $^{36}O_2$ ratio from the partial pressure curves shown in Fig. 2c, we used electrolysis of the same isotope $H_2{}^{16}O$ to calibrate the response of the system. Basically, we removed the injection port, connected the electrolysis flask directly to the gas sampling valve, and monitored the generation of H_2 and $^{36}O_2$ over time as shown in Fig. 2d. Comparing the curves in Fig. 2c with the calibration curves in Fig. 2d, we can conclude that both photocatalytic water splitting and electrolysis give a similar H_2 to $^{36}O_2$ ratio. As the ratio of H_2 to $^{36}O_2$ from electrolysis is 2:1, we reached the conclusion that we also had a ~2:1 ratio of H_2 to $^{36}O_2$ in CoO phootcatalytic water splitting.

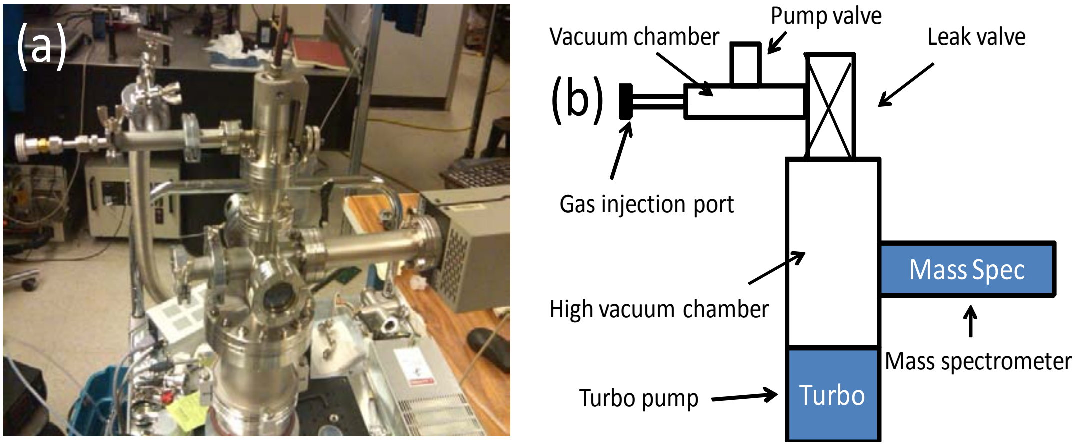

Figure 9. Picture and schematic of the home-built gas analyzing system.

The strong H_2 response of the RGA to the injection of air (Fig. 2c) is called the anomalous effects in pressure measurements of hydrogen with ionization gauges and residual gas analyzers (http://wwwold.jlab.org/hydrogen/talks/Redhead.pdf). The volume concentration of H_2 in air is only 0.000055%. However, H_2 is a predominate residual gas in high vacuum systems. This is because: (1) H_2 is very difficult to pump out, especially with a turbo-molecular pump in our case; (2) H_2 can be desorbed from the vacuum walls, i.e. from the surface or body of metals. H_2 also causes serious problem in its vacuum measurement because of the so-called electron stimulated desorption (ESD) of hydrogen ions or neutrals from the layer of adsorbed hydrogen on the grid of the ionization gauge or the ion-source of the RGA.

(5) Electrochemical Impedance Measurement

In order to measure band edge positions (or flatband potentials) of CoO nanocrystals as well as CoO micro-powder, thin film electrodes of nanocrystals and powders were fabricated on fluorine-doped tin oxide (FTO) conducting glasses (Hartford Glass Co., sheet resistance of 7 Ω/□). CoO nanocrystal thin film was obtained by drying nanocrystal aqueous suspension from the synthesis beaker on a FTO glass. The same procedure was applied to CoO powders, except that the powders had to be dispersed in water first. The dried thin films were then annealed at 510 °C for 4 hrs in an Ar environment. Copper wires were used as contacts to the film, the areas of thin film electrodes were ~1 cm^2. The electrolyte was 0.4 M Na_2SO4 solution (pH 6.8) deaerated by bubbling N_2 for at least 25 min before each experiment. A platinum line was used as a counter electrode, and Ag/AgCl (in 3.0 M NaCl solution) was used as a reference electrode connected to Na_2SO4 solution by a salt bridge. Electrochemical impedance spectroscopy (EIS) measurements were carried out using a 263A Princeton Applied Research (PAR) potentialstat/galvanostat in combination with a PAR M5210 lock-in amplifier. Both the potentialstat and the lock-in amplifier were controlled by a computer using PowerSuite software version 4.7. The potential was scanned between 0.6 and 2.1 V with five different modulation frequencies.

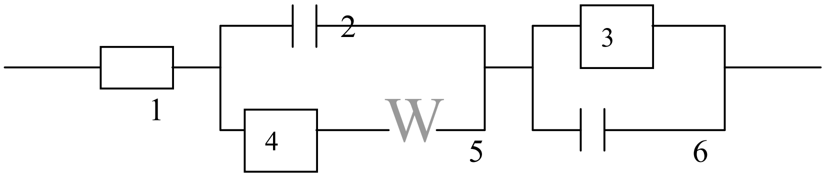

Figure 10. Equivalent circuit used to obtain capacitance of CoO nanocrystal and powder films. 1, Electrolyte resistance; 2, CoO/electrolyte interface capacitance; 3, CoO resistance; 4, charge-transfer resistance; 5, Warburg impedance, and 6, CoO capacitance.

The thin film/electrolyte systems were modeled with the equivalent circuit shown in Fig. S10. The value for each component was obtained with ZSimpWin software using complex nonlinear least square fitting (CNLS). All the potentials reported here are relative to the reference electrode Ag/AgCl unless otherwise stated. Potential conversion between Ag/Cl and NHE is given by: E(NHE) = E(Ag/AgCl) + 0.212 V. The obtained CoO capacitances were used for the Mott-Schottky plots in Fig. 3c.